Journal of Materials Chemistry A

Accepted Manuscript

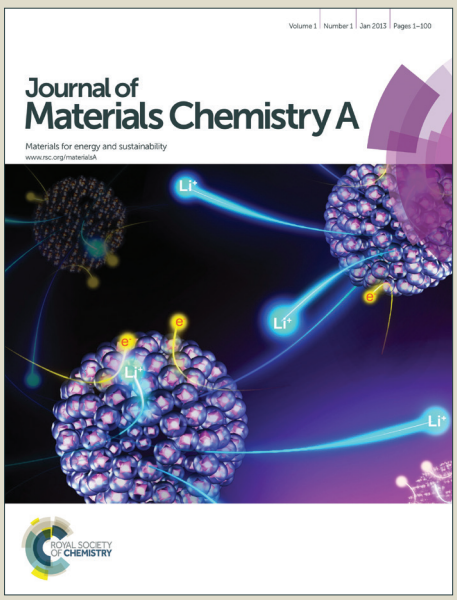

ROYAL SOCIETY OF CHEMISTRY

www.rsc.org/materialsA

Ag/AgCl plasmonic cubes with ultrahigh activity as advanced visible-light photocatalysts for photodegrading dyes

Z. Y. Lin, J. Xiao, J. H. Yan, P. Liu, L. H. Li and G. W. Yang *

State Key Laboratory of Optoelectronic Materials and Technologies, Nanotechnology Research Center, School of Physics & Engineering, Sun Yat-sen University, Guangzhou 510275, Guangdong, P. R. China

*Corresponding author: stsygw@mail.sysu.edu.cn

Abstract

Among numerous visible-light photocatalysts, plasmonic structure is a promising photocatalyst in photodegradation and energy generation. Ag/AgCl composite as an alternative visible-light photocatalyst has attracted extensive interests, however, the syntheses have many visible flaws, e.g. high temperature environment, various templates or additives, demanding complicated synthetic procedures and causing impurities in final products, and so on. For these issues, herein, we reported that a simple, facile, rapid and green technique has been developed to synthesize the Ag/AgCl heterostructured cubes using a one-step process of laser irradiation in liquid for the first time. The fabricated Ag/AgCl cubes possess some active {111} facets and a high visible-light utilization efficiency induced by the localized surface plasmon resonance (SPR) from Ag/AgCl heterostructure. As the plasmonic photocatalysts, these Ag/AgCl cubes exhibited excellent photodegrading performance for dyes molecules of methyl orange, Rhodamine B and methylene blue, and the photodegradation rates were about 0.268, 0.057, and 0.094 min^{-1}, which are much higher than that of commercial Ag_3PO_4 by a factor of 29.8, 3.8 and 6.7, respectively. The high photo-stability of the Ag/AgCl cubes was also demonstrated. The SPR-mediated photocatalytic mechanism was proposed to address the ultrahigh activity of Ag/AgCl heterostructure as an advanced visible-light photocatalyst. These results showed the broad applicability of the developed technique for accessing new plasmonic photocatalyst with high-performance.

Introduction

Methyl orange (MO), Rhodamine B (RhB) and methylene blue (MB) are the most common organic pollutants in water pollution, which are weakly degradable and even carcinogenic.[1] Photocatalytic degradation based on the conventional titanium dioxide (TiO_2) has thus attracted broad attention since 1972.[2] However, only the UV fraction of the solar energy (generally 4%) is utilized in the TiO_2-based photodegradation because of the wide bandgap of TiO_2.[3]Therefore, there has been a growing interest in developing visible-light photocatalysts for several decades. Ag/AgCl composite as an alternative visible-light photocatalysts has recently attracted considerable attention due to multifunction.[4] Ag/AgCl heterostructure has been found applications not only for visible-light photodegradation, but also water photolysis,[5] photoelectric detection,[6] surface enhanced Raman scattering (SERS),[7] and bacterial disinfection,[8] thanks to the positively synergistic effect between metal Ag species and semiconductor AgCl.

Although multifarious approaches have been designed elaborately to synthesize Ag/AgCl composites, most of them are unfortunately complicated and time-consuming because at least two-step processes, e.g., synthesis of AgCl followed by deposition of Ag species, are involved.[9-37] In the AgCl preparation, ion-exchange reactions between different Ag^+ cation sources[9-13] and Cl^- anion sources[9-23] take place. In many cases, external capping agents (PVP[9] and PVA[24]) are required as stabilizers. Whereafter, the Ag^+ ions in AgCl lattice would be reduced and deposited onto AgCl surface by photoreduction,[10,11,14,16,18,32-34] electron-beam reduction,[20, 35] or chemical

reduction.[9,10,24,35-37] In conclusion, these reported syntheses are usually multi-steps and time-consuming, and some of them are complicated and require high temperature environment. Moreover, the final products are basically on the scale of several micrometers, and they are easily polluted on account of the need of external reducing agents and capping agents.

For these issues above, in this contribution, we report a simple, facile, rapid and green route to synthesize unique Ag/AgCl heterostructured cubes within one-step using a novel and well-designed process involving laser ablation in liquid (LAL).[38] In previous reports,[39,40] Yan *et al.* reported the first synthesis of AgCl nanocubes by laser ablation of a silver target in NaCl solution. Although Ag nanoclusters were proved to coexist in the solution, they were believed to be isolated from AgCl cubes. Ag/AgCl composites have never been prepared by LAL so far. To the best of our knowledge, Ag/AgCl cubes are prepared by the one-step LAL procedure in this work for the first time. The as-synthesized AgCl cubes with abundant small Ag nanoparticles tends to expose some high-energy {111} facets, accounting for more active sites for photodegradation. We demonstrate that the as-synthesized Ag/AgCl composites manifest high visible-light utilization efficiency and excellent photocatalytic performance in the degradation of MO, RhB and MB under visible-light irradiation, especially for MO. Thus SPR-mediated photocatalytic mechanism is proposed. Furthermore, the Ag/AgCl plasmonic photocatalyst is resistant to photo-corrosion and exhibits prominently high photo-stability after four recycling experiments. Therefore, these investigations show the applicability of LAL for the development of new

photocatalysts.

Experimental section

Ag/AgCl cubes synthesis. The experiments are carried out by a LAL process. Typically, $AgNO_3$ solution (20 mM) is prepared in advance by dissolving 40.8 mg $AgNO_3$ (Alfa Aesar, 99.9+%, metals basis, powder) into 12 mL deionized water in a 18 mL glass bottle. About 30.0 mg AgCl powder (Alfa Aesar, 99.997%, metals basis, powder) is added into $AgNO_3$ solution to form the suspension. After sonicating for 5 min, the suspension is kept stirring with a magnetic stirrer in the dark. Then, a third harmonic produced by a Q-switched Nd:YAG laser device with a wavelength of 355 nm, laser pulse power of 20 mJ, pulse width of 10 ns, and repeating frequency of 50 Hz is focused by a lens (100 mm) into the suspension for 20 min. As a result, a brick-red colloid solution is synthesized. Finally, the samples are collected by centrifugation, washed with deionized water repeatedly.

Ag/AgCl cubes characterization. The morphology and composition of the products are recorded by thermal FE environment scanning electron microscope (SEM, Quanta 400, FEI Company) and energy dispersive X-ray spectrometer (EDS, INCA, Oxford Company). Transmission electron microscopy (TEM) and energy dispersive X-ray (EDX) elemental mapping analysis are acquired by using an FEI Tecnai G2 F30 transition electron microscope with a field-emission gun. The structure of the products are identified by an X-ray diffractometer (XRD, D/MAX-2200, Rigaku) under a voltage of 40 V and a current of 26 mA, and recorded with a speed of

1^{o} min^{-1}. UV-visible diffuse reflectance spectra (DRS) is recorded on a UV-VIS-NIR spectrophotometer (Lambda950, PerkinElmer Company) using $BaSO_4$ as a reference.

Photocatalytic reaction. MO, RhB and MB solution are selected as the target organic pollutants to probe the visible-light-driven photocatalytic performance of the samples. 20.0 mg of the sample is added to 20 mL of MO solution (10 mg L^{-1}) in a test-tube, and then stirred vigorously in the dark for 30 min to establish an adsorption-desorption equilibrium of MO molecules on the photocatalysts before exposing to the visible-light irradiation. The photodegradation test is conducted in a photochemical reactions instrument (QIQIAN-III, Qiqian Company) using a 500W Xe arc lamp with a 420 nm cutoff filter as the light source to simulate the sunlight. Aliquots of solution (2.0 mL) are drawn from the test-tube at respective irradiation time intervals (3 min), and then centrifuged at 5000 rpm for 10 min to remove the photocatalysts. The supernate is transferred to a quartz cuvette for measuring their absorption spectra under a UV-VIS-NIR spectrophotometer (Lambda900, PerkinElmer Company). Photodegradation of RhB and MB is also conducted in the same way. In order to judge the photocatalytic performance of the samples, equal amounts of commercial visible-light photocatalyst Ag_3PO_4 powders (Alfa Aesar, 99%, powder) are introduced for comparison. Self-photolysis of dyes molecules is carried out by visible-light irradiation of the solutions without any samples. In addition, Ag/AgCl samples after the first cycle photodegradation of MO are collected by centrifuging and washing for subsequent three recycling tests to verify the

photo-stability of the samples. SEM, EDS, XRD and DRS of the recycled samples are carried out, as well.

Results and Discussion

Synthesis and characterization of Ag/AgCl cubes. The Ag/AgCl cubes growth mechanism can be described as Scheme 1 and reaction equations (1) - (4).

$$AgCl_p \xrightarrow{Ag^+, h\upsilon} AgCl_f \quad (1)$$

$$Ag^+ + AgCl_f \xrightarrow{HT} Ag^+Cl^- / AgCl_c \quad (2)$$

$$Ag^+Cl^- / AgCl_c \xrightarrow{h\upsilon} e^- + h^+ \quad (3)$$

$$Ag^+Cl^- / AgCl_c + e^- \xrightarrow{AgCl_c, h\upsilon} Ag / AgCl \quad (4)$$

Herein, $AgCl_p$, $AgCl_f$, $Ag^+Cl^-/AgCl_c$ and Ag/AgCl represent the original AgCl powder, AgCl fragment, Ag^+Cl^- electric bilayer capped AgCl core and end product Ag/AgCl cube. And HT means heat temperature.

AgCl is a kind of photo-sensitive materials with wide bandgap,[41] and it would become more sensitive in presence of adsorbed Ag^+ ions on its surface due to the charge-transfer transitions.[42] When a 355 nm pulsed laser irradiates AgCl powders in $AgNO_3$ solution, these powders would absorb the high energy of laser and fragmentize,[38] as equation (1) and Scheme 1(a) show. During the laser irradiation, the transient temperature of the irradiation areas would become extremely high,[38] which not only increase the reaction rate, but also promote the dissolution of AgCl in water. According to the Le Chatelier's principle,[22] the solubility of AgCl would be larger at high temperature, and more Cl^- ions would appear in the solution due to the excess of

Ag^+ ions. Therefore, the growth of AgCl crystals would be terminated with Cl^- ions, making it negatively charged. As is described in Equation (2) and Scheme 1(b), the free Ag^+ ions would be absorbed onto the surface of AgCl core to form a Ag^+Cl^- electric bilayer and inhibit the AgCl core growing very fast. The growth of Ag nanoparticles on the AgCl cube surface can be described as Equations (3) - (4) and Scheme 2(c-e). Because of the point ionic defects and electron traps,[4] abundant e^--h^+ pairs would be generated on the surface of AgCl core under the UV laser irradiation, and Ag^+ ions in the surrounding would be reduced to Ag seeds on the surface of AgCl cube under the catalysis of AgCl[39]. Note that Ag nanoparticles can be fragmentized by the 355 nm laser effectively.[43] Thus, the generated Ag nanoparticles on the surface of AgCl would be relatively small.

Typical SEM images of the sample are shown in Fig. 1(a). Clearly, we can see that many nanoparticles with diameter of about 30 nm are distributed densely on the surfaces of the cubes with edge length in the range of 200-400 nm, which could be named as quasi-nanocubes. Meanwhile, the EDS spectrum exhibited in Fig. 1(b) shows that the sample is composed of Ag and Cl elements, and the Si peak originates from the silicon wafer as a substrate. The atomic ratio of Ag and Cl of the sample is about 4.74:1, which suggests that Ag element content is more than Cl content in the sample. However, the exact ratio of Ag: Cl (related to that of Ag: AgCl) could not be obtained because AgCl is sensitive to electron beam[23, 39, 41] and Ag^+ ions in AgCl lattice would be reduced and deposited on the surface of AgCl, which increases the ratio of Ag: Cl in the sample. To demonstrate the elements distribution of the sample,

EDX elemental mapping analysis is carried out. Typical TEM image and STEM image are shown in Fig. 1(c) and (d), respectively. In Fig. 1(e-f), we can see that the orange and cyan colors represent the mapping of Ag and Cl elements, respectively. Through careful observation, we can find out that Fig. 1(e) is almost identical to Fig. 1(d), indicating Ag element spreads over all the area of the sample. And the distribution of Cl element in Fig. 1(f) has obvious boundary in the shape of cube. Moreover, the dark areas of Fig. 1(f) correspond to the bright ones of Fig. 1(e), stating that Ag nanoparticles are deposited on the surface of the sample, which weakens the signal intensity of Cl element in the corresponding areas. Thus we believe that the sample is consisted of external dense Ag nanoparticles and internal cubic Ag and Cl compound, maybe AgCl. Unfortunately, high resolution TEM (HRTEM) and selected area electronic diffraction (SAED) images cannot be acquired to analyze the phase composition of the sample because the high-energy electron beam easily destroys AgCl and Ag crystals.[1, 33] Therefore, XRD characterization was chosen to verify the phase composition.

The XRD pattern of the sample is shown in Fig. 1(g). We can clearly see that the coexistence of the cubic phase of AgCl with lattice constant a = 0.55491 nm (PDF #31-1238) and the cubic phase of Ag with lattice constant a = 0.40864 nm (PDF #04-07839). In detail, the peaks at 2θ = 27.64°, 32.08°, 46.02°, 54.66°, 57.32° and 67.20° belong to the (111), (200), (220), (311), (222) and (400) facets of AgCl, respectively. And the peaks at 2θ = 35.92°, 43.94° and 64.22° belong to the (111), (200) and (220) facets of Ag, respectively. Compared with the standard data, all the

diffraction peaks 2θ of AgCl cubes and Ag nanoparticles show a left-shift of about 0.2°, which may be due to the strong interaction between AgCl cubes and Ag nanoparticles. Obviously, the peaks of Ag are broader than those of AgCl, which suggests that Ag particles are much smaller than AgCl cubes. It is noteworthy that the diffraction peaks of Ag are apparent, which is different from other reports,[5, 36] stating Ag nanoparticles in the sample is abundant. These results indicate that the sample is consisted of Ag species and AgCl crystal.

Therefore, it can be believed that the dark and light areas of Fig. 1(c) correspond to Ag nanoparticles and AgCl cube, respectively. At this point, the heterostructured nature of Ag/AgCl cubes is substantiated.

It is worth mentioning that the diameter of Ag nanoparticles in Fig. 1(c) is in the range of 40-100 nm, which is at odds with the SEM result. That is also because of the sensitivity of AgCl to electron beam. The work voltage of about 300 kV in TEM observation is much higher than that of 3 kV in SEM observation. Therefore, the pre-existing Ag nanoparticles would grow much faster in TEM observation. In addition, as the signs of red arrows in SEM and TEM images show, the Ag nanoparticles are always in the shape of semi-sphere instead of sphere, which demonstrates that the Ag nanoparticles and AgCl cubes are in good contact with each other. Observe carefully, we can find out that the AgCl cube is not a standard cube. The corners of the AgCl cubes are always smooth, not generally sharp, marked with the signs of green arrows in Fig, 1(a) and Fig. 1(c). It may be because of the selective growth of different facets in AgCl crystals.[44,45] As is simulated in Fig. 1(h), in our case,

the corners smoothing of cubic crystals may originates from the exposure of {111} and {110} facets. Taking the three main XRD peaks of AgCl crystal into consideration, the diffraction peak intensity ratio $I_{(111)}/I_{(200)}$ of about 0.7 is larger than that of 0.5 for the standard data, and $I_{(220)}/I_{(200)}$ of about 0.4 is smaller than that of 0.5 for the standard data. These suggest that the AgCl crystals grow mainly along the <100> directions, while some {111} facets are exposed. Therefore, it is plausible to consider that the corners smoothing of the as-prepared Ag/AgCl cube is due to the exposure of AgCl {111} facets. In detail, we believe that the geometry-modifying effect of Ag^+ ions results in the selective growth of different facets in AgCl crystals, similar to Cl^- [28] and PVP.[37] Cl^- ions in the {100} facets are saturated by Ag^+ ions, and the {100} facets of AgCl crystals possess the minimum surface energy. The {111} planes with ridge-and-valley topography are thus exposed with plenty of low-coordinate surface Cl^- ions with many dangling bonds, which resulting in the higher surface energy. Cl^- ions on the {111} facets possessing many dangling bonds can combine with Ag^+ ions in the solution due to the electrostatic interaction, and then change the relative surface energy.[46] In our case, the relative surface energy of {111} and {100} facets becomes smaller, but the surface energy of {111} facet is still larger than that of {100} facet. Therefore, it is believed that the geometry-modifying effect makes some {111} facets expose while AgCl crystals grow mainly along the <100> directions.

Based on the discussion above, we can conclude that the small Ag/AgCl heterostructured cubes with dense and small Ag nanoparticles, and some exposing high-energy AgCl {111} facets were fabricated by the one-step LAL procedure.

The LAL process is believed to be novel and well-designed because of the following reasons. Firstly, external Ag^+ is used to sensitize AgCl, which enhances the preparation efficiency. Secondly, an excess of Ag^+ is chosen as stabilizer, instead of organics PVP and PVA. It keeps the products clean, which is good for photocatalytic performance. Thirdly, the exposure of some high-energy {111} facets, resulting from the geometry-modifying effect of Ag^+ ions, provides more active sites for photocatalysis. Fourthly, in many situations, Ag particles are deposited onto the AgCl surface by reducing the Ag^+ in AgCl crystal lattice. Additional recombination centers would be brought to weaken the e^--h^+ pair separation ability. An external Ag^+ source may avoid this problem. Last but not least, the wavelength of 355 nm is selected, instead of others, to guarantee a small scale of Ag particles.

Photocatalytic performance of Ag/AgCl cubes. The visible-light-driven photodegradation performance of the Ag/AgCl cubes for MO, RhB and MB is shown in Fig. 2-3 and Table 1. As is shown in Fig. 2(a), the absorbance of MO at 464 nm (the characteristic absorption peak) decreases rapidly during the photocatalysis process. In our case, the relative concentrations of MO solution is determined by the relative absorbance based on the Beer-Lambert law of C = k'A, herein, k' is the absorption constant, A and C are the absorbance and concentration at time t, respectively. Especially, C_{-30} and C_0 are the concentrations of MO solution before and after a 30-min adsorption-desorption equilibrium. The Ag/AgCl cubes degrade a 10 mg L^{-1} MO solution in about 24 min, as is shown in Fig. 2(b). In the cases of the photocatalytic experiments using RhB and MB as target pollutants, the conducting

parameters are the same as that of MO, as is shown in Fig. 2(c-f). The characteristic absorption peaks of RhB and MB are set as 554 and 664 nm, respectively. Commercial visible-light photocatalyst Ag_3PO_4 is used for comparison under the same conditions. In addition, MO, RhB and MB solutions without the presence of the Ag/AgCl cubes can hardly be degraded under visible-light irradiation, as is shown in Fig. 2(b, d, f). These results thus indicate that the degradation has nothing to do with the self-photolysis of dye molecules.

Assuming that the degradation process obeys the first-order kinetics ($C = C_0e^{-kt}$, k is the photodegradation rate), the plots of $-\ln(C/C_0)$ as a function of the irradiation time t are shown in Fig. 3(a-c). The relevant parameters including adsorptivity r, photodegradation rate k and correlation coefficient R are collected into Table 1.We can see that the photodegradation behaviors of the Ag/AgCl cubes for MO, RhB and MB obey the first-order kinetics indeed, and the photodegradation rates are about 0.268, 0.057, and 0.094 min^{-1}, which are higher than that of Ag_3PO_4 by a factor of 29.8, 3.8 and 6.7, respectively. Therefore, the Ag/AgCl cubes have the highest photodegradation rate for MO among MO, RhB and MB, but they have the lowest adsorptivity for MO. Possible explanations are put forward as follows.

Since AgCl crystals are terminated with Cl^- ions, the Ag/AgCl cubes are usually negatively charged.[4] Because MO, RhB and MB dyes are anionic, zwitterionic and cationic organics, respectively, shown in Fig. 3(d), adsorption capacities of the Ag/AgCl cubes for MO, RhB and MB are quite different (7.06% for MO, 9.93% for RhB and 40.38% for MB). Although MO dyes are absorbed least, the

photodegradation rate for MO is the largest. We can find out that the maximum absorption peaks of RhB and MB show significant blue shifts in Fig. 2(c, e) while that of MO keeps unchanged in Fig. 2(a). This is related to the degradation pathways of the Ag/AgCl cubes for different dyes molecules. There are two degradation pathways of MO, RhB and MB molecules: N-dealkylation and chromophore cleavage. The significant blue shifts of RhB absorption peaks are due to the formation of a series of N-dealkylation intermediates.[47] Typical absorption curve of MB solution always shows two characteristic peaks located at 667 and 610nm, which originate from the absorption of MB monomers and dimers, respectively.[9] The blue shift of MB absorption peaks are due to the desynchrony degradation of MB monomers and dimers and the formation of N-dealkylation intermediates.[48] The absorption peaks of MO solution do not show any shift, which indicates that no degradation intermediates form in the degradation process. Therefore, the as-prepared Ag/AgCl can photodegrade MO with a higher rate. In addition, MO molecules are of azo configuration, and the complications[18] of Ag^+ with nitrogen in MO molecules would also promote the degradation.

In order to understand the possible visible-light-driven photocatalytic mechanism of as-prepared Ag/AgCl cubes, the light absorption property of the sample is analyzed by UV-visible diffuse reflectance spectra (UV-vis DRS). As is shown in Fig. 4(a) (black line), the sample exhibits three absorption peaks around 235, 298 and 500 nm. In detail, the absorption peaks of 235 and 298 nm below 400 nm in the UV light area are ascribed to the wide bandgap of AgCl, whose indirect and direct bandgaps are

3.28 and 5.28 eV, respectively.[49] Note that, a great absorption of visible-light of the sample in the wavelength range from 400 to 700 nm can be attributed to the localized surface plasmon resonance (SPR) from Ag/AgCl heterostructure.[4, 10] In fact, the phenomenon that the maximum absorbance of visible-light is much higher than that of UV-light has rarely been reported in the literatures.[4, 7, 10] Therefore, this result suggests that the sample has a strong absorption capacity of visible-light. In addition, the SPR wavelength of Ag nanoparticles is believed to locate between 350 and 450 nm, independent of the size, which is slightly different from the result of our case. In our studies, the red shift of the SPR wavelength is ascribed to two reasons as follows. The first reason is that small interparticle spacing decreases the SPR frequency,[31] and the second one is that the dielectric constant of AgCl is larger than that of water (2.7 $>$1.33), which can compensate the restoring force of Ag nanoparticles more and decrease the SPR frequency.[41] Therefore, it is believed that the as-prepared Ag/AgCl cubes exhibit excellent visible-light utilization efficiency.

Recycling photodegradation experiments for MO are carried out for four times to test the stability and recyclability of the sample. As is shown in Fig. 4(b), the sample does not show significant decrease in degradation performance after four cycles. The XRD pattern of the four times recycled samples (red line) is almost identical to the original pattern (black line), shown in Fig. 4(c). It can be further proved by the normalized diffraction intensity histograms (black and red) and the corresponding diffraction intensity ratio histogram (blue) in Fig. 4(c). It can be seen that most of the diffraction intensity ratio is nearly equal to 1, except for AgCl (400) facet diffraction

peak which is not the main diffraction peak. SEM images and corresponding EDS spectrum of the recycled samples in Fig. 4(d-f) also confirmed that the morphology and elementary composition almost keep unchanged. Note that the Ag content is a little larger than the original sample because of the photo-sensitivity of AgCl. Further studies indicate that the recycled samples possess a strong absorption capacity of visible light, as well, shown in Fig. 4(a) (red line). Neither the morphology nor phase composition is changed. So the sample keeps performing high visible light absorption and excellent photocatalysis. The little weakening of the photocatalytic performance may be due to the small aggregation of Ag/AgCl cubes. At this point, it is reasonable to believe that the as-prepared Ag/AgCl cubes are resistant to photo-corrosion and exhibit prominently high photo-stability.[34,50]

SPR-mediated photocatalytic mechanism. The excellent visible-light photocatalytic activity of Ag/AgCl cubes is attributed to the positively synergistic effect between Ag nanoparticles and semiconductor AgCl crystal, which could be named as SPR-mediated photocatalytic mechanism, shown in Scheme 2. The Fermi level of Ag nanoparticle locates in the bandgap of AgCl crystal and is higher than that of AgCl. When Ag nanoparticles are directly deposited onto the surface of AgCl crystal, a Schottky barrier would spontaneously be established at the interface to form a common Fermi level for equilibration. Therefore, under the visible-light irradiation, a lot of hot electrons would come into being, and the Fermi level of Ag would rise greatly to above the conduction band of AgCl by the SPR effect. Meanwhile, some e^--h^+ pairs would be generated in AgCl owing to its photo-sensitivity. As a result of

the high visible-light utilization efficiency and the photo-sensitivity of AgCl crystals, Ag/AgCl cubes possess a high e^--h^+ pairs generation efficiency.

Due to the strong polarization of surface Cl^- ions, the SPR-induced strong electric-field enhancement and the SPR-induced localized heating effect, the hot electrons would transfer to the conduction band of AgCl very quickly ($\leq 150\,fs$).[10] Because of the near field effect of SPR,[4] a blocking layer at the interface between Ag and AgCl is undesirable, which would hinder the energy transferring from Ag to AgCl. The as-synthesized Ag/AgCl cubes can meet this requirement because neither external capping agents nor reducing agents are needed in the LAL process in this research. Therefore, Ag/AgCl cube can act as an outstanding e^--h^+ pairs separation promoter.

The separated e^--h^+ pairs can react with atoms, molecules and ions in the surrounding to generate reactive species, and degrade the dye molecules further. Superoxide anion radicals ($\cdot O_2^-$), hydrogen peroxide radicals (H_2O_2), hydroxyl radicals ($\cdot OH$), active chlorine (Cl^0), hypochlorous acid (HOCl), and even holes (h^+) may be responsible for the degradation.[23,26,34,37, 51] All the possible reactions can be listed as follows.

$$Ag / AgCl + h\upsilon \longrightarrow e^- + h^+ \quad (5)$$

$$e^- + O_2 \longrightarrow \bullet O_2^- \quad (6)$$

$$e^- + 2H^+ + \bullet O_2^- \longrightarrow H_2O_2 \quad (7)$$

$$e^- + H_2O_2 \longrightarrow \bullet OH + OH^- \quad (8)$$

$$h^+ + OH^- \longrightarrow \bullet OH \quad (9)$$

$$h^+ + H_2O \longrightarrow \bullet OH + H^+ \quad (10)$$

$$h^+ + Cl^- \longrightarrow Cl^0 \quad (11)$$

$$2Cl^0 \longrightarrow Cl_2 \quad (12)$$

$$Cl_2 + H_2O \longrightarrow HOCl + H^+ + Cl^- \quad (13)$$

$$2HOCl \longrightarrow O_2 + 2H^+ + 2Cl^- \quad (14)$$

$$h^+, \bullet O_2^-, H_2O_2, \bullet OH, Cl^0, HOCl + dyes \longrightarrow De\,\mathrm{Pr}\,od. \quad (15)$$

Herein, "DeProd." means Degradation Products. Cl^0 originating from Cl^- in the AgCl lattice would be reduced to Cl^- again by dyes molecules, and combines with Ag^+ to form AgCl crystal and keep Ag/AgCl cubes stable.

$$Ag^+ + Cl^- \longrightarrow AgCl \quad (16)$$

It's believed that the more active sites photocatalysts possess, the higher photocatalytic activity they would show.[52] Thanks to the small scale of the Ag/AgCl cubes, a large specific surface area can be obtained to provide many adsorption sites for dyes molecules. And exposing AgCl {111} facets with high surface energy are helpful for offering more active sites for the photodegradation.

According to the analyses and discussions above, we can conclude that a high e^--h^+ pairs generation efficiency, an ultrafast e^--h^+ pairs separation rate and a large active sites quantity result in an ultrahigh photocatalytic activity of Ag/AgCl plasmonic cubes.

Conclusion

In summary, Ag/AgCl heterostructured cubes are prepared by the one-step LAL procedure for the first time. It is a novel and well-designed method because $AgNO_3$

can act as sensitizer, stabilizer and geometry-modifier of AgCl crystal, and the selective laser wavelength of 355nm can guarantee the small scale of Ag nanoparticles. The as-synthesized Ag/AgCl cubes expose some active {111} crystal facets and possess a high visible-light utilization efficiency due to the localized SPR from Ag/AgCl heterostructure, and thus they can be named as plasmonic photocatalysts. Meanwhile, these Ag/AgCl cubes exhibit excellent photocatalytic performance in the degradation of MO, RhB and MB undergoing the SPR-mediated photocatalytic mechanism. Neither morphology nor phase composition of the sample is changed after four recycling experiments. The Ag/AgCl cubes still keep high visible light absorption and excellent photocatalytic performance. Thanks to their prominently high photo-stability, it is possible to apply them in practice.

Acknowledgements. The National Basic Research Program of China (2014CB931700) and the State Key Laboratory of Optoelectronic Materials and Technologies of Sun Yat-sen University supported this work.

References

1 H. Chen, L. Xiao and J. H. Huang, *Materials Research Bulletin* , 2014, **57**, 35-40.

2 A. Fujishima and K. Honda, *Nature*, 1972, **238**, 37-38.

3 A. Naldoni, M. Allieta, S. Santangelo, M. Marelli, F. Fabbri, S. Cappelli, C. L. Bianchi, R. Psaro and V. D. Santo, *J. Am. Chem. Soc.*, 2012, **134**, 7600-7603.

4 P. Wang, B. B. Huang, X. Y. Qin, X. Y. Zhang, Y. Dai, J. Y. Wei and M. H. Whangbo, *Angew. Chem. Int. Ed.*, 2008, **47**, 7931-7933.

5 Z. Z. Lou, B. B. Huang, X. Y. Qin, X. Y. Zhang, H. F. Cheng, Y. Y. Liu, S. Y. Wang, J. P. Wang and Y. Dai, *Chem. Commun.*, 2012, **48**, 3488-3490.

6 L. Han, Z. K. Xu, P. Wang and S. J. Dong, *Chem. Commun.*, 2013, **49**, 4953-4955.

7 F. L. Cui, M. H. Zhai, K. L. Wu, N. Yu and Z. H. Wang, *Micro & Nano Letters*, 2014, **9**, 297-301.

8 V. Gopinath, S. Priyadarshini, N. M. Priyadharsshini, K. Pandian and P. Velusamy, *Mater. Lett.*, 2013, **91**, 224-227.

9 C. H. An, S. Peng and Y. G. Sun, *Adv. Mater.*,2010, **22**, 2570-2574.

10 Y. X. Tang, Z. L. Jiang, G. C. Xing, A. R. Li, P. D. Kanhere, Y. Y. Zhang, T. C. Sum, S. Z. Li, X. D. Chen, Z. L. Dong and Z. Chen, *Adv. Funct. Mater.*,2013, **23**, 2932-2940.

11 D. L. Chen, M. N. Liu, Q. Q. Chen, L. F. Ge, B. B. Fan, H. L. Wang, H. X. Lu, D. Y. Yang, R. Zhang, Q. S. Yan, G. S. Shao, J. Sun and L. Gao, *Applied Catalysis B: Environmental*, 2014, **144**, 394-407.

12 H. Gatemala, C. Thammacharoen and S. Ekgasit, *CrystEngComm.*, 2014, **16**, 6688-6696.

13 S. N. Zhang, H. F. Tian, S. J. Zhang, L. M. Song, X. Q. Wu, J. Y. Ye and Q. W. Wei, *Chem. Eng. J.,* 2014, **240**, 548-553.

14 G. Q. Wang, H. Mitomo, Y. Matsuo, N. Shimamoto, K. Niikura and K. Ijiro, *J. Mater. Chem. B*, 2013, **1**, 5899-5907.

15 M. C. Li, H. Yu, R. Huang, F. Bai, M. Trevor, D. D. Song, B. Jiang and Y. F. Li, *Nanoscale Research Letters*, 2013, **8**, 442-447.

16 P. Hu, X. L. Hu, C. J. Chen, D. F. Hou and Y. H. Huang, *CrystEngComm.*, 2014, **16**, 649-653.

17 H. Daupor and S. Wongnawa, *Applied Catalysis A: General*, 2014, **473**, 59-69.

18 L. Han, P. Wang, C. Z. Zhu, Y. M. Zhai and S. J. Dong, *Nanoscale*, 2011**, 3**, 2931-2935.

19 M. Husein, E. Rodil and J. Vera, *Langmuir*, 2003, **19**, 8467-8474.

20 E. V. Formo, W. J. Fu, A. J. Rondinone and S. Dai, *RSC Advances*, 2012, **2**, 9359-9361.

21 T. S. Dhas, V. G. Kumar, V. Karthick, K. J. Angel and K. Govindaraju, *Spectrochimica Acta Part A: Molecular and Biomolecular Spectroscopy*, 2014, **120**, 416-420.

22 A. A. Kulkarni and B. M. Bhanage, *ACS Sustainable Chem. Eng.*, 2014, **2**, 1007-1013.

23 S. Majumder, B. Naskar, S. Ghosh, C. H. Lee, C.-H. Chang, S. P. Moulik and A. K. Panda, *Colloids and Surfaces A: Physicochem. Eng. Aspects*, 2014, **443**, 156-163.

24 J. Song, J. Roh, I. Lee and J. Jang, *Dalton Trans.*, 2013, **42**, 13897-13904.

25 P. Wang, B. B. Huang, Z. Z. Lou, X. Y. Zhang, X. Y. Qin, Y. Dai, Z. K. Zheng and X. N. Wang, *Chem. Eur. J.*, 2010, **16**, 538-544.

26 L. H. Ai, C. H. Zhang and J. Jiang, *Applied Catalysis B: Environmental*, 2013, **142**, 744-751.

27 Y. G. Xu, H. Xu, H. M. Li, J. Yan, J. X. Xia, S. Yin and Q. Zhang, *Colloids and Surfaces A: Physicochem. Eng. Aspects*, 2013, **416**, 80-85.

28 Z. Z. Lou, B. B. Huang, X. C. Ma, X. Y. Zhang, X. Y. Qin, Z. Y. Wang ,Y. Dai and Y. Y. Liu, *Chem. Eur. J.*, 2012, **18**, 16090-16096.

29 Y. Y. Li and Y. Ding, *J. Phys. Chem. C.*, 2010, **114**, 3175-3179.

30 Y. Nakajima, Q. L. Jin and H. Tada, *Electrochem. Comm.*, 2008, **10**, 1132-1135.

31 P. F. Hu, Y. L. Cao, D, Z. Jia, Q. Li and R. L . Liu, *Sci. Rep.*, 2014, **4**, 4153.

32 L. H. Dong, D. D. Liang and R. C. Gong, *Eur. J. Inorg. Chem.*, 2012, **19**, 3200-3208.

33 R. F. Dong, B. Z. Tian, C. Y. Zeng, T. Y. Li, T. T. Wang and J. L .Zhang, *J. Phys. Chem. C.*, 2013, **117**, 213-220.

34 B. Z. Tian, R. F. Dong, J. M. Zhang, S. Y. Bao, F. Yang and J. L. Zhang, *Applied Catalysis B: Environmental* , 2014, **158**, 76-84.

35 W. S. Choi, G. Y. Byun, T. S. Bae and H. J. Lee, *ACS Appl. Mater. Interfaces*, 2013, **5**, 11225-11233.

36 D. L. Chen, S. H. Yoo, Q. S. Huang, G. Ali and S. O. Cho, *Chem. Eur. J.* 2012, **18**, 5192-5200.

37 B. Cai, J. Wang, S. Y. Gan, D. X. Han , Z. J. Wu and L. Niu, *J. Mater. Chem. A*, 2014, **2**, 5280-5286.

38 G. W. Yang, *Prog. Mater. Sci.*, 2007, **52**, 648-698.

39 Z. J. Yan, G. Compagnini and D. B. Chrisey, *J. Phys. Chem. C*, 2011, **115**, 5058-5062.

40 C. B. Dong, Z. J. Yan, J. Kokx, D. B. Chrisey, C. Z. Dinu, *Applied Surface Science*, 2012, **258**, 9218-9222.

41 X. C. Ma, Y. Dai, L. Yu, Z. Z. Lou, B. B. Huang and M. H. Whangbo, *J. Phys. Chem. C*, 2014, **118**, 12133-12140.

42 S. Glaus and G. Calzaferri, *J. Phys. Chem. B*, 1999, **103**, 5622-5630.

43 C. H. Bae, S. H. Nam and S. M. Park, *Applied Surface Science*, 2002, **197,** 628-634.

44 B. Z. Tian and J. L. Zhang, *Catal. Surv. Asia*, 2012, **16**, 210-230.

45 M. S. Zhu, P. L. Chen and M. H. Liu, *J. Mater. Chem.*, 2011, **21**, 16413-16419.

46 X. C. Ma, Y. Dai, J. B. Lu, M. Guo and B. B. Huang, *J. Phys. Chem. C*, 2012, **116**, 19372-19378.

47 X. F. Hu, T. Mohamood, W. H. Ma, C. C. Chen and J. C. Zhao, *J. Phys. Chem. B*, 2006, **110**, 26012-26018.

48 C. Yogi, K. Kojima, N. Wada, H. Tokumoto, T. Kakai, T. Mizoguchi and H. Tamiaki, *Thin Solid Films*, 2008, **516**, 5881-5884.

49 S. Glaus and G. Calzaferri, *Photochem. Photobiol. Sci.*, 2003, **2**, 398-401.

50 X. J. Li, D. L. Tang, F. Tang, Y. Y. Zhu, C. F. He, M. H. Liu, C. X. Lin and Y. F. Liu, *Materials Research Bulletin*, 2014, **56**, 125-133.

51 J. X. Shu, Z. H. Wang, G. Q. Xia, Y. Y. Zheng, L. H. Yang and W. Zhang, *Chem. Eng. J.*, 2014, **252**, 374-381.

52 Q. H. Liang, Y. Shi, W. J. Ma, Z. Li and X. M. Yang, *Applied Catalysis A: General*, 2013, **455**, 199-205.

Table1. Relevant parameters (r, k and R) about photodegradation of MO, RhB and MB.

photocatalyst	dye	Adsorptivity (r) /%	Photodegradation rate (k) /min^{-1}	Correlation coefficient R
Ag/AgCl	MO	7.06	0.268	0.989
	RhB	9.93	0.057	0.999
	MB	40.38	0.094	0.996
Ag_3PO_4	MO	10.72	0.009	0.996
	RhB	7.14	0.015	0.987
	MB	8.26	0.014	0.995

Figure Captions

Scheme 1. Schematic illustration of the formation of Ag/AgCl cubes in the process of laser irradiation in liquid.

Scheme 2. Schematic illustration of the energy band structure of Ag/AgCl heterostructure and the photocatalytic dyes degradation process.

Figure 1. (a) SEM images of Ag/AgCl cubes at low magnification and at high magnification (the insert, scale bar: 100nm). (b) The corresponding EDS spectrum and elements analysis (the insert) of Ag/AgCl cubes. (c) TEM image of Ag/AgCl cubes. (d-f) EDX elemental mapping analysis of Ag/AgCl cubes. (g) The corresponding XRD pattern of Ag/AgCl cubes. (h) Schematic illustration of {100}, {110} and {111} facets of a cubic crystal.

Figure 2. (a), (c) and (e) Typical UV-vis spectral changes of MO, RhB and MB solution in the presence of Ag/AgCl cubes. The insert of (a) is the detailed views of absorbance at 18, 21, 24 min. (b), (d) and (f) The relative concentrations plots of MO solution with the presence of Ag/AgCl cubes or Ag_3PO_4, and without any photocatalysts (referred as blank).

Figure 3. (a-c) The plots of $-\ln(C/C_0)$ *vs* t with the presence of Ag/AgCl cubes or Ag_3PO_4 in MO, RhB and MB solution. (d) The molecular structures of MO, RhB and MB molecule.

Figure 4. (a) UV-vis absorption spectra of Ag/AgCl cubes before and after four recycling experiments. (b) Recycling experiments of Ag/AgCl cubes in photodegradation of MO. (c) XRD patterns of Ag/AgCl cubes before (black line) and after (red line) four recycling experiments, and normalized diffraction peaks intensity histograms before (black) and after (red) four recycling experiments, and diffraction peaks intensity ratio histogram (blue).

Scheme 1

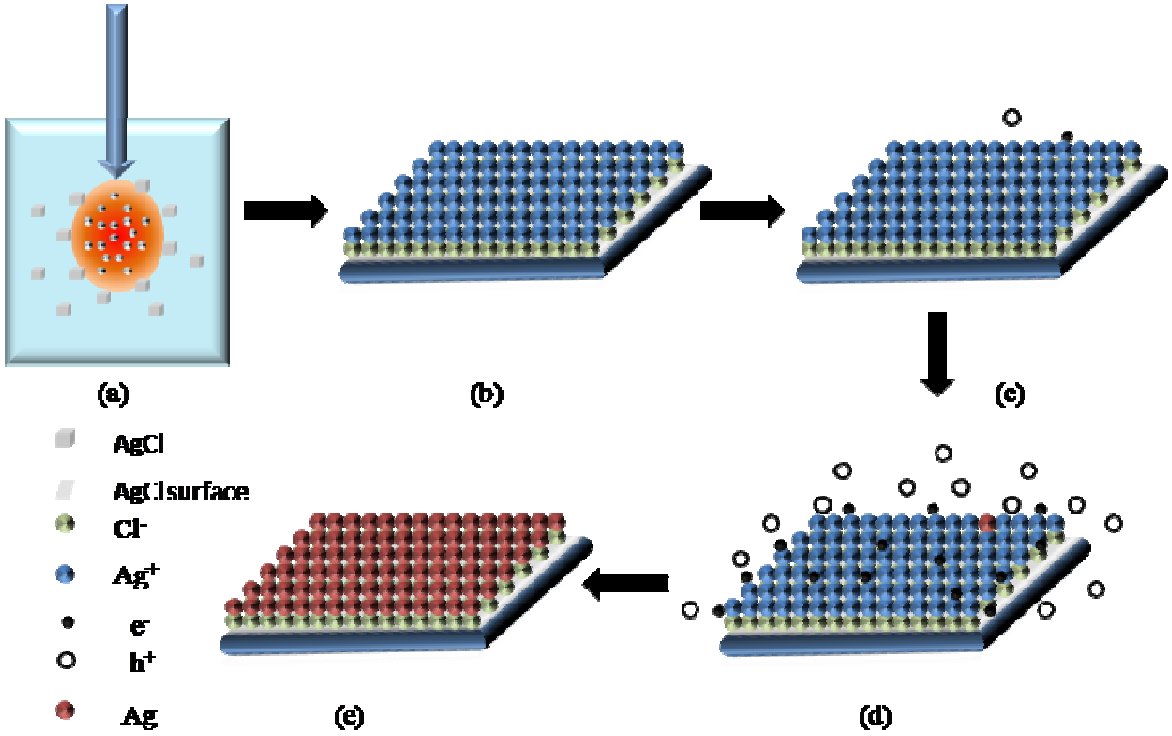

Scheme 2

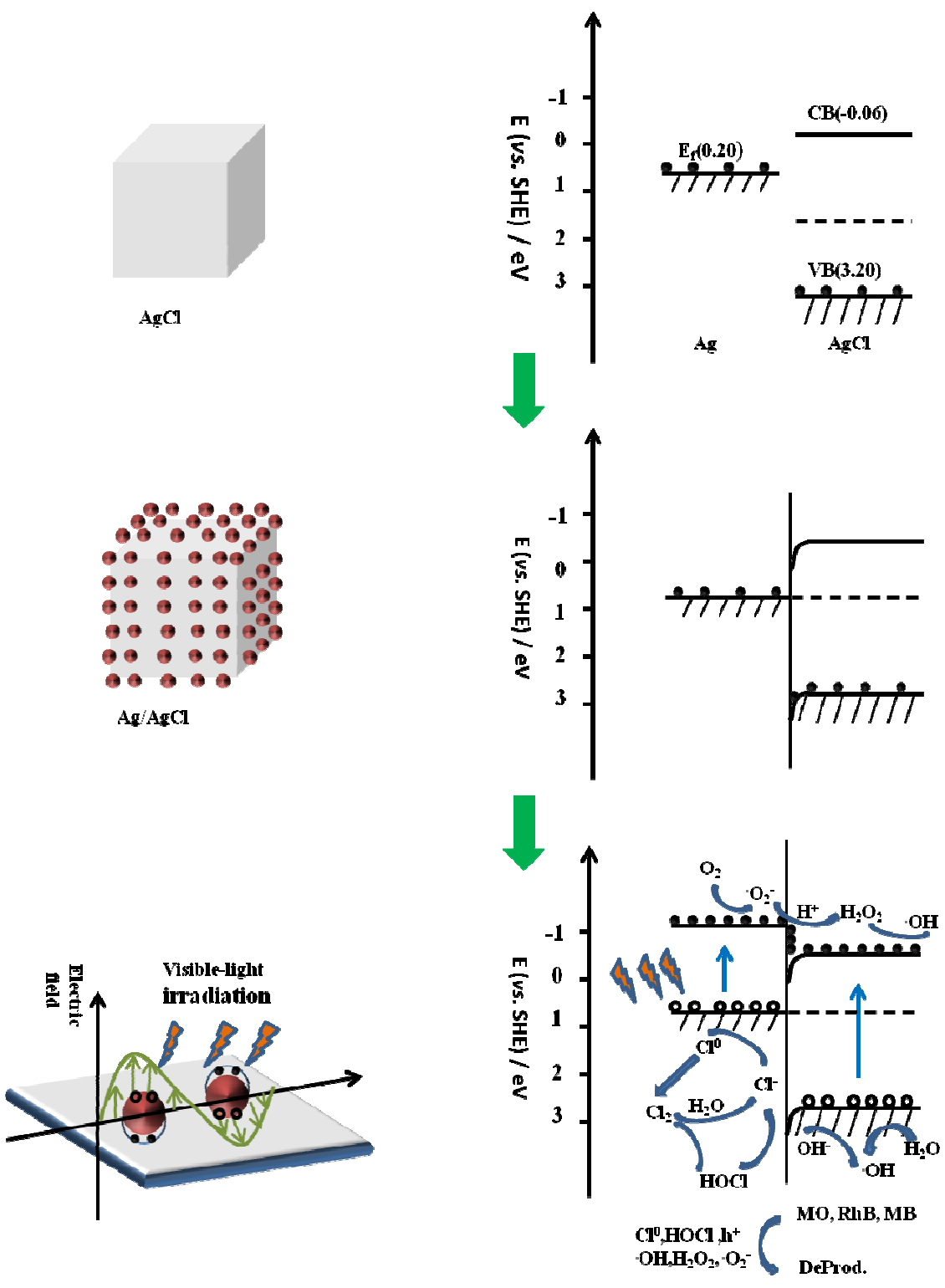

Figure 1

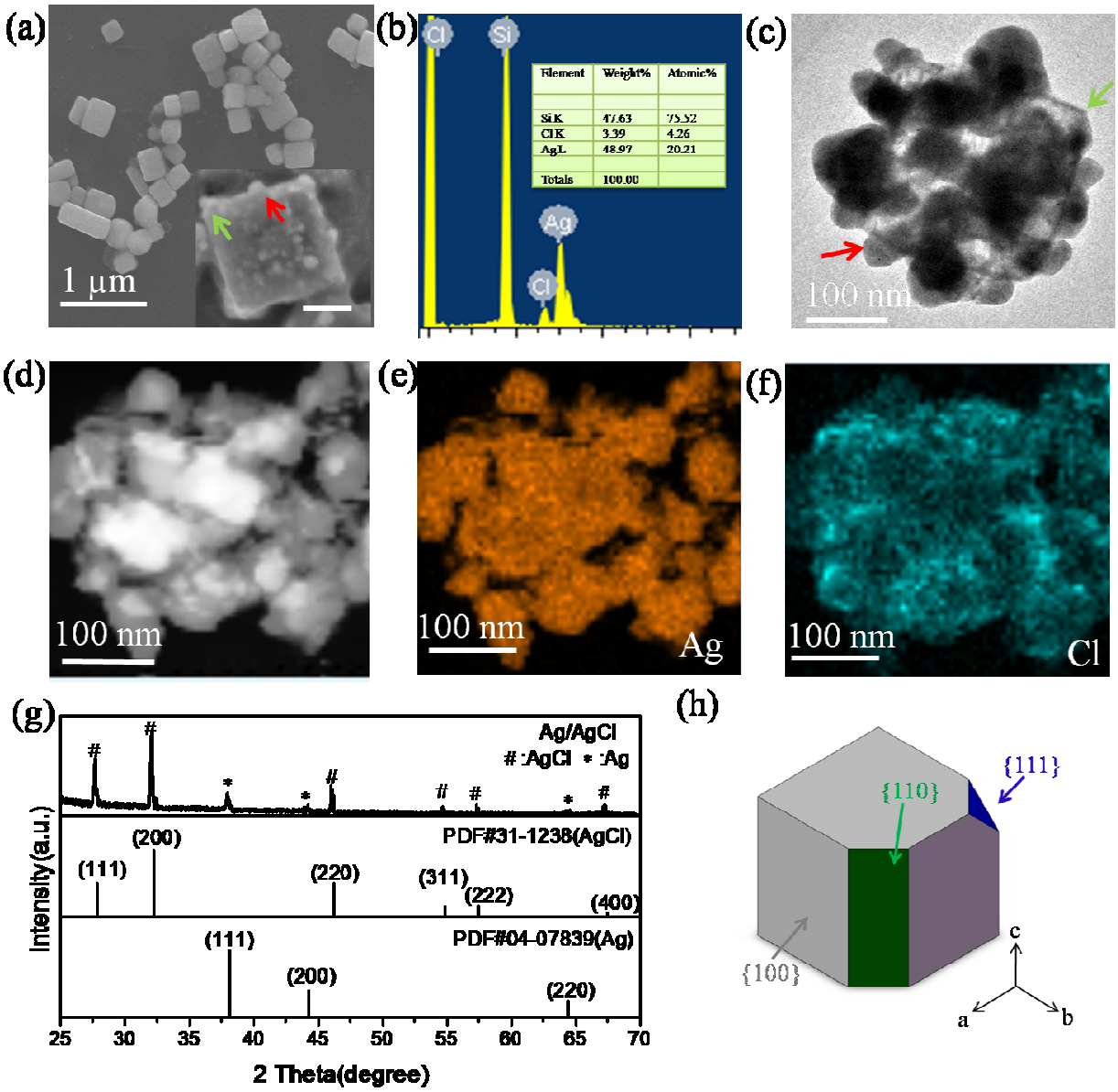

Figure 2

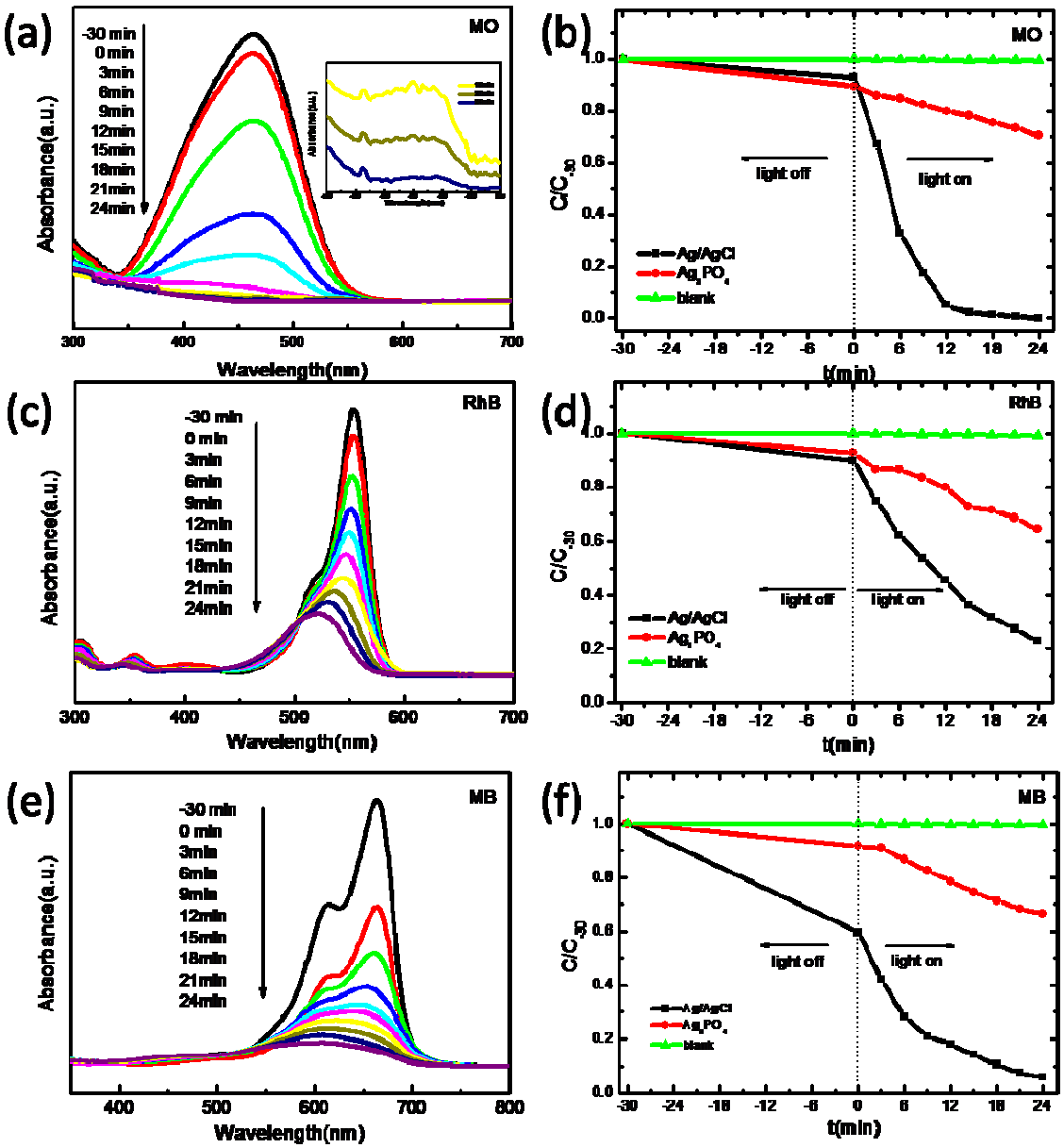

Figure 3

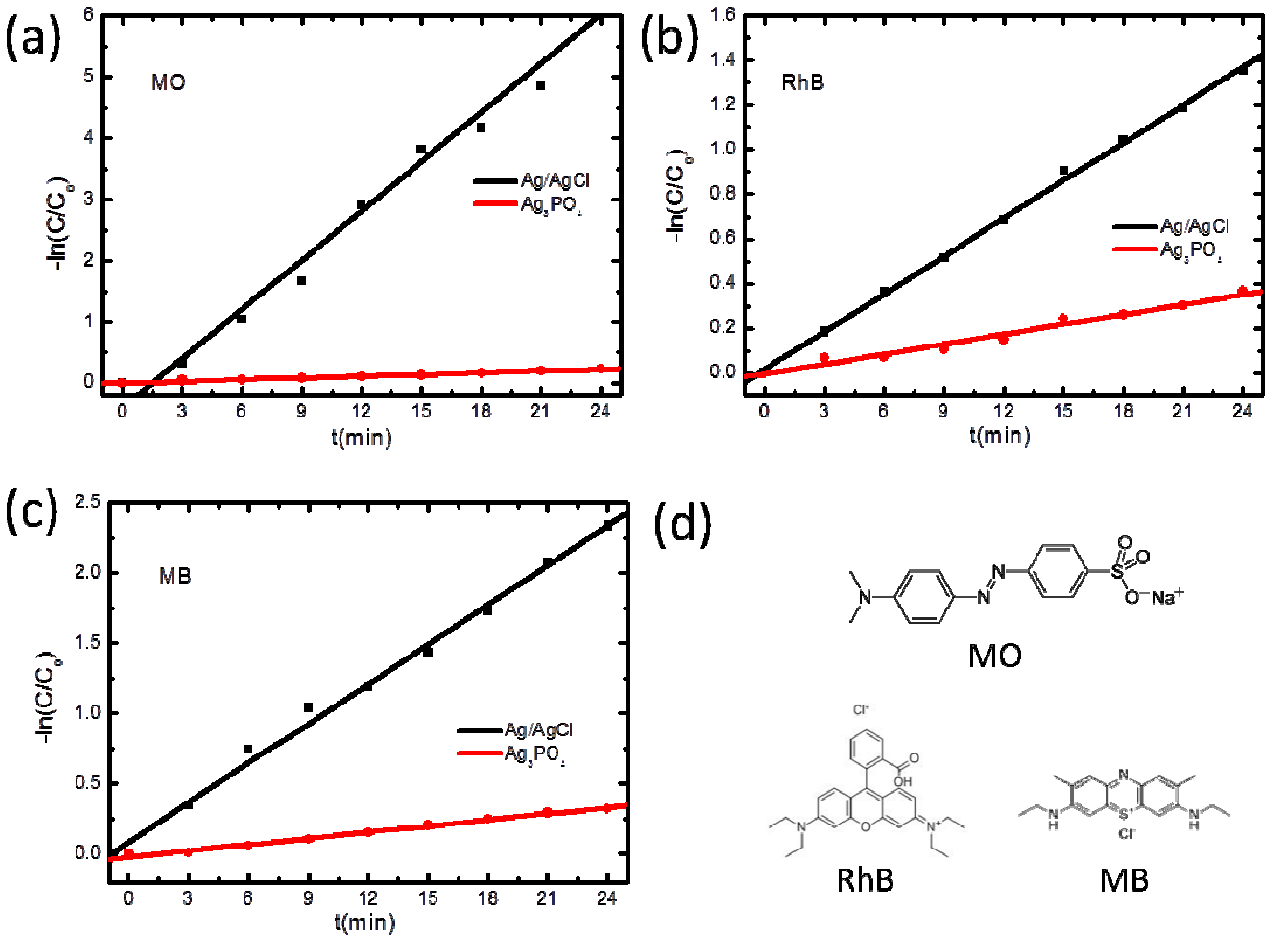

Figure 4

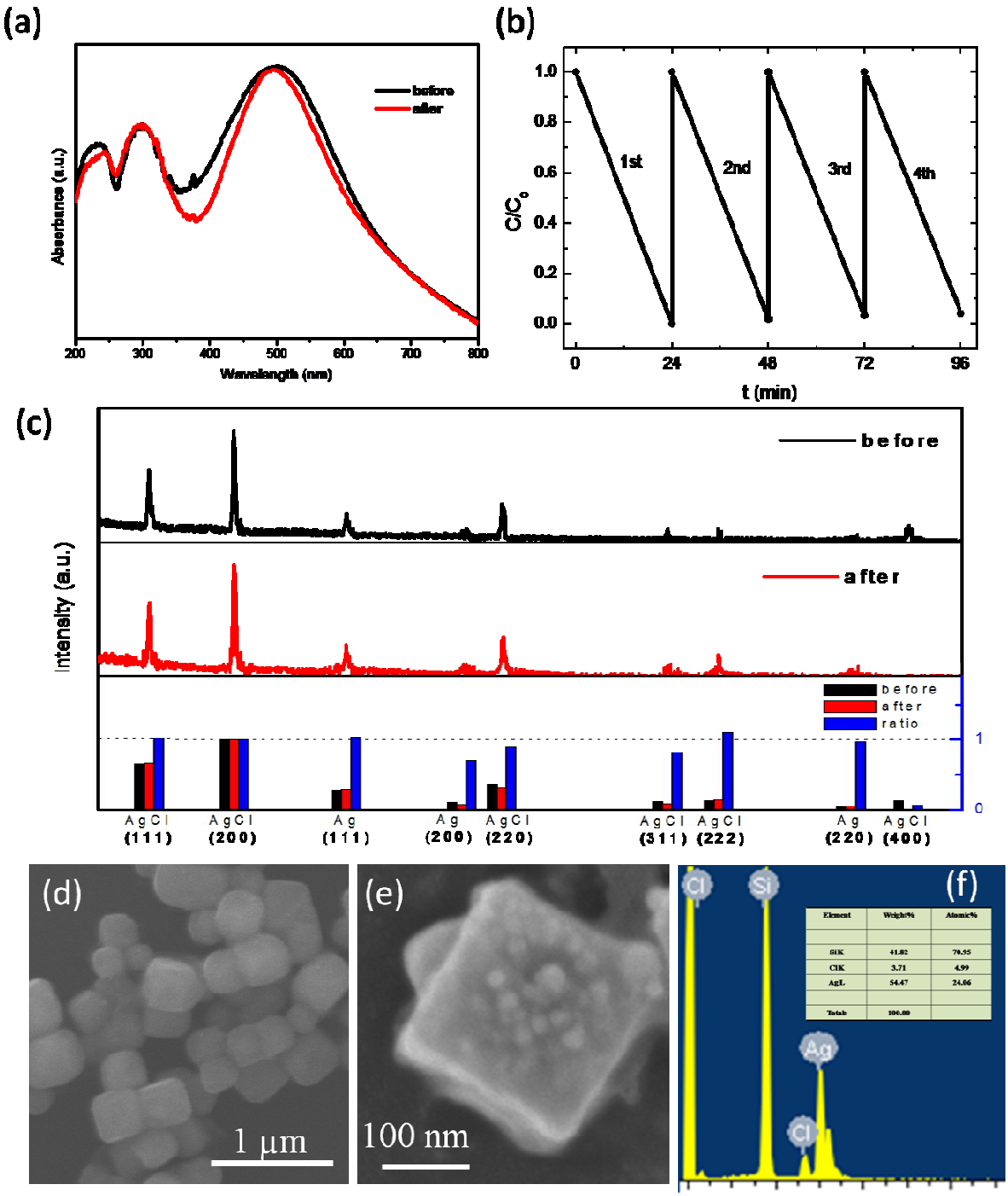

A table of contents entry

Ag/AgCl heterostructured nanocubes have been fabricated and used as advanced visible-light photocatalysts for photodegrading dyes.